Complementary Analysis of Thermal Transition Multiplicity of Hen Egg-White Lysozyme at Low pH Using X-ray Scattering and Scanning Calorimetry

Mitsuhiro Hirai,* Shigeki Arai, and Hiroki Iwase

Department of Physics, Gunma University, 4-2 Aramaki, Maebashi 371-8510, Japan

Received: May 20, 1998; In Final Form: November 2, 1998

In this present paper we present a new method of small-angle X-ray scattering (SAXS) data analysis (called the TMA method) to examine multiplicity of structural transition of denaturation processes of proteins. The TMA method gives us a molar fraction of spatial-conformational-state and an indication of deviation from the two-state structural transition hypothesis in a structural transition process. Using this method we have successfully compared a spatial-conformational-state transition observed by SAXS with a thermodynamic-microstate transition observed by differential scanning calorimetry (DSC) in the thermal denaturation process of hen egg-white lysozyme (HEWL) at the pH range of 2.4−3.1. The TMA method is able to dissect spatial-conformational-state transition multiplicity depending on structural hierarchy. We have found that the thermal structural transition of HEWL is well-characterized mostly in terms of two different spatial-conformational-state transitions in the tertiary and intramolecular structures. Upon heating, the transition-midpoint temperature of the spatial-conformational-state transition of the tertiary structure mostly agrees with that of DSC, while the transition-midpoint temperature of the intramolecular structure greatly differs from that of DSC. The tertiary structural transition essentially obeys the two-state transition feature with a sharp critical temperature in comparison with the intramolecular structural transition. When the pH is lowered from 3.1 to 2.4, the former transition tends to shows a maximum deviation from the two-state transition feature around the transition temperature. On the other hand, the intramolecular structural transition proceeds continuously with a relatively large deviation in the whole temperature range measured at all pH values. The present results obtained by the TMA method essentially agree with our previous report using standard SAXS analyses in HEWL system at different pH range of 7.0−1.2, and would afford us further aspects to discuss experimental evidences with theoretical models of protein folding, such as nucleation-collapse models.

Introduction

How a polypeptide chain attains its native conformation has been attracting significant scientific concerns as an important biological fundamental problem. Numerous studies on the protein folding and unfolding have been carried out through the use of various methods such as calorimetry, fluorescence, circular dichroism, nuclear magnetic resonance, X-ray scattering, and mutation techniques.[1,2] From late 1960's many intensive studies on the thermal denaturation of proteins in solution have been carried out using mainly differential scanning calorimetry (DSC) to clarify the thermodynamic basis of stability of the conformational states of proteins.[3−8] Now it is generally accepted that unfolding transitions of single-domain proteins under equilibrium conditions are usually two-state ones where only fully folded and unfolded states are populated.[9,10]

The folding-and-unfolding transition of hen egg-white lysozyme (HEWL) had also been considered to show a highly cooperative two-state process and not to take an intermediate state in the transition process.[11,12] The studies using nuclear magnetic resonance (NMR) and circular dichroism (CD) have clarified that HEWL consists of the two structural domains which are stabilized with different kinetics and involve parallel alternative pathways in folding such as distinct folding-domains.[13−16] A recent study using a precise scanning calorimeter has also observed the presence of intermediates during the thermal denaturation of HEWL at low pH.[17] Recently, by using small-angle X-ray scattering (SAXS) and DSC, we have shown the characteristics of the thermal denaturation process of HEWL at pH 1.2, 3.9, and 7.0 depending on structural hierarchy in comparison with the case of α-lactalbumin at pH 7.[18] Namely, the tertiary structural transition of HEWL above pH ∼4 proceeds as a two-state transition with a sharp transition point around the onset temperature observed by DSC, while at pH 1.2 this transition proceeds rather gradually. On the other hand, the intramolecular structural change starts from lower temperature than the above transition temperature and proceeds gradually at all pH values. Our wide-angle neutron scattering study supports the above results.[19] However, we have recognized the necessity of a new method of SAXS-data analysis to give results comparable with DSC data more directly since in the above report[18] we carried out only standard analyses of SAXS data (estimation of radius of gyration, distance distribution function, Kratky plot, and Porod plot).

Under the theoretical bases of thermodynamics, DSC data is well-known to serve us a heat capacity function $C(T)$ of macromolecules which afford thermodynamic functions such as calorimetric enthalpy $H(T)$ and Gibbs free energy $G(T)$, and we can estimate molar fractions of the thermodynamic microstates by using the advanced algorithms for the analysis of

* Author to whom correspondence should be addressed. Phone: INT+81 272-20-7554. Fax: INT+81 272-20-7551 or 7552. E-mail: hirai@sun.aramaki.gunma-u.ac.jp.

10.1021/jp982315v CCC: $18.00
Published on Web 01/05/1999

DSC curves.[20−22] A thermodynamic state at some temperature is defined by an ensemble of some microstates at equilibrium, namely by the canonical partition function of the whole system $Z(T)$. This is the basis of DSC analyses. A recent excellent theoretical work using a new statistical thermodynamic formalism has clearly shown that thermodynamic microstates of proteins are strongly coupled with protein structures.[23] On the other hand, scattering techniques, such as small-angle X-ray and neutron scattering methods, evidently have a great advantage for determining directly the spatial-conformational states of macromolecules in solutions since scattering functions observed reflect those of an ensemble of multiple spatial-conformations of the solute macromolecules, especially at the denatured state. Despite such an advantage, in many cases scattering techniques have been used to estimate only a few structural parameters, such as the radius of gyration and the Kratky plot, for discussion of spatial-conformational-state transitions in protein folding-and-unfolding studies.[24,25]

To make a direct comparison of SAXS data with DSC data we have developed a new method of SAXS data analysis which enables us to discuss multiplicity of spatial-conformational-state transitions in denaturation and renaturation processes of proteins. Using this method we have successfully clarified multiplicity of spatial-conformational-state transitions in the thermal transition of HEWL at the narrow pH range 3.1−2.4, which depends on both structural hierarchy and pH. We selected this pH range because our previous study suggests that the thermal transition feature of HEWL will change significantly at this pH range.[18]

Experimental Procedures

Materials. The samples used were hen egg-white lysozyme purchased from Sigma Chemical Co. Sodium citrate buffer solvents from Wako Pure Chemical Industries, Ltd., were used. The lysozyme was solubilized in citrate buffer solvents with the same ionic strength adjusted by adding NaCl ($[Na^+] = 0.2$ M). pH values of the solutions were determined to be pH 2.4, 2.8, and 3.1 by using a Digital pH Meter HM-60V from TOA Electronics Ltd. The lysozyme concentrations of the solutions served for the present experiments were all 10% w/v.

Small-Angle X-ray Scattering Measurements. SAXS experiments were carried out with a small-angle scattering spectrometer[26] installed at the 2.5 GeV storage ring in the Photon Factory, Tsukuba, Japan. A one-dimensional position-sensitive proportional counter detected the scattering intensity. The wavelength used was 1.49 Å, and the sample-to-detector distance was 60 cm. A sample cell composed of a pair of mica windows with 1 mm path length and containing sample solutions was place in a thermostated cell-holder with a precision below 0.1 °C. The temperature of the samples was elevated stepwise from 20 to 80 °C with the temperature interval of 2.5−5.0 °C, which was monitored by using a thermocouple device attached directly to the sample cell. The exposure time for one measurement was 4 min and the integrated exposure time for one sample was 72 min.

Methods of Scattering Data Analyses. After correction of the scattering data by subtracting background, the scattering curves $I(q)$ were analyzed as follows. The distance distribution function $p(r)$ was obtained by the Fourier transform of the scattering intensity $I(q)$ as

$$p(r) = \frac{2}{\pi}\int_0^\infty rq/(q)\sin(rq)\,dq \qquad (1)$$

where q is the magnitude of scattering vector defined by $q = (4\pi/\lambda)\sin(\theta/2)$ (θ, the scattering angle; λ, the wavelength). The $p(r)$ function depends on the particle shape and on the intraparticle scattering density distribution. To reduce the Fourier truncation effect in the calculation of the $p(r)$ function, the extrapolation of the small-angle data sets using the least-squares method in the Guinier plot ($\ln(I(q))$ vs q^2) and the modification of the scattering intensity as

$$I'(q) = I(q)\exp(-kq^2) \qquad (2)$$

(k is the artificial damping factor) were done. The maximum diameter D_{max} of the particle was estimated from the $p(r)$ function satisfying the condition $p(r) = 0$ for $r > D_{max}$. As the use of the Guinier approximation for determining the radius of gyration R_g is subject to inherent systematic errors caused by concentration or aggregation effect,[27] we used the Glatter's method to reduce such artifacts for estimating R_g values, as given by

$$I_{total} = \int_0^{D_{max}} p(r)\,dr \qquad (3)$$

and

$$R_g^2 = \int_0^{D_{max}} p(r)r^2\,dr / \int_0^{D_{max}} p(r)\,dr \qquad (4)$$

Equation 3 was used for normalization of the $p(r)$ functions. The Kratky plot ($q^2I(q)$ vs q) for the scattering angle region higher than the Porod slope region[28] was also used to examine a certain rigidity of polymer chains since this plot reflects the short-range interactions acting along the chain from neighbor to neighbor such as bond forces and hindrance of rotation.[29−33]

Differential Scanning Calorimetry Measurements. DSC measurements were done using a differential scanning calorimeter PC DSC7 from the Perkin−Elmer Co. To compare SAXS data with DSC data directly, the lysozyme solutions of the DSC measurements (10% w/v, at pH 2.4, 2.8, and 3.1) were prepared under the same conditions used for the scattering measurements. The. Scanning rate was 5 °C/min. We measured thermograms in the temperature range 10−85 °C.

Results

Standard Analyses of Scattering Data. Figure 1 shows the temperature dependence of the scattering curves $I(q)$ of the lysozyme solutions: 1(a), 1(b), and 1(c) correspond to pH 3.1, pH 2.8, and pH 2.4, respectively. As is well-known, the structural information contained in the scattering curve $I(q)$ depends on the observed q range. In the present sample system, the scattering curve $I(q)$ below $q \sim 0.1$ Å^{-1} corresponds to the real-space distance over ∼60 Å, reflecting mostly the interparticle spatial-correlation of HEWL molecules. The $I(q)$ in the q range of ∼0.1−0.2 Å^{-1}, corresponding to the real-space distance of ∼30−60 Å, reflects mostly the molecular shape and the dimension, namely the tertiary structure of HEWL molecule. The $I(q)$ in the q range of ∼0.3−0.6 Å^{-1}, corresponding to the real-space distance of ∼10−20 Å, reflects the intramolecular structure such as the interdomain correlation and the intramolecular polypeptide arrangement. The scattering curve in the q range of ∼0.3−0.5 Å^{-1} initiates a gradual change from the lowest temperature of 20 °C at all pH values, whereas the change of the scattering curve in the q range of ∼0.1−0.2 Å^{-1} starts from a higher temperature depending on pH. The above difference suggests that the intramolecular structure follows a multi-state transition and that the tertiary structure does a two-state transition. In addition, the fast increase of the scattering intensity below $q \sim 0.1$ Å^{-1} occurs simultaneously with the

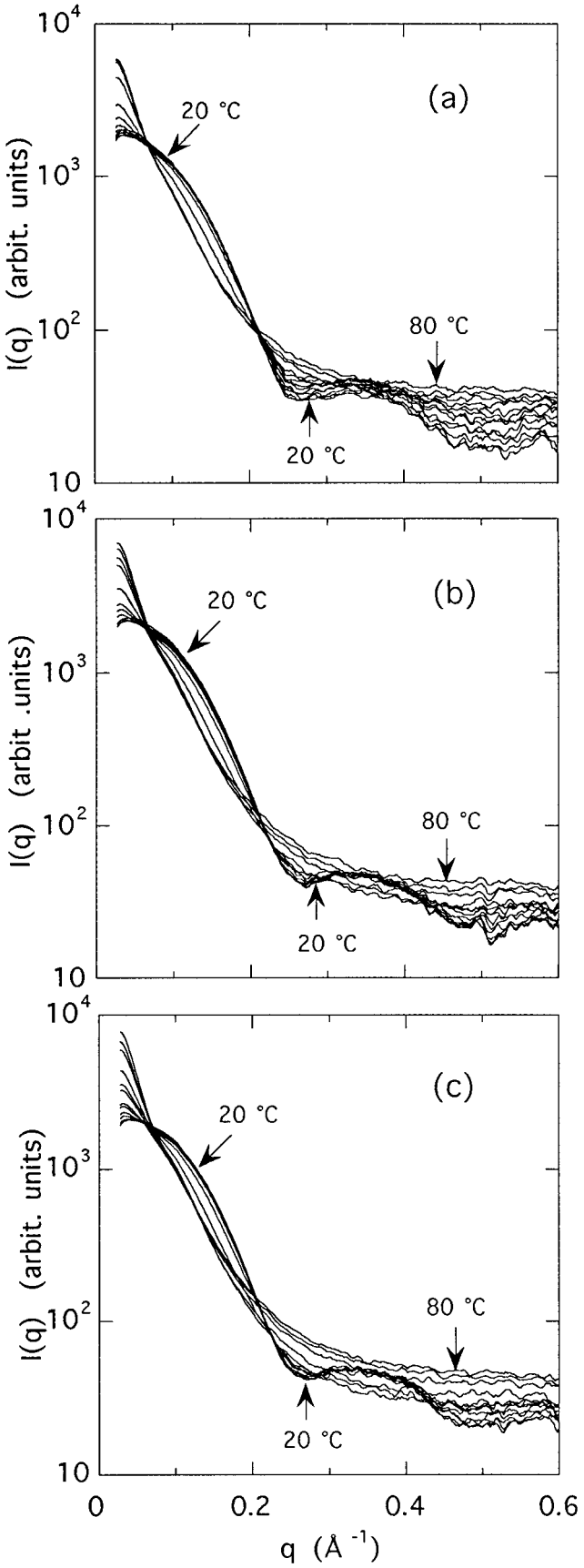

Figure 1. Temperature dependence of the scattering curves of the hen egg-white lysozyme solutions (10% w/v) in citrate buffer at different pH values ($[Na^+] = 0.2$ M). (a) at pH 3.1; (b) at pH 2.8; (c) at pH 2.4. The temperature was elevated stepwise from 20 to 80 °C. The changes of the scattering curves for each 5 °C rise in temperature are presented.

marked change of the scattering curve at ~0.1−0.2 Å^{-1}, indicating that the collapse of the tertiary structure causes an aggregation of HEWL molecules.

In Figures 2, 3, and 4 we can confirm the above structural changes in detail. The Kratky plot well reflects short-range interactions and local conformations in polymer chains.[28−32] In Figure 2 the Kratky plot above $q \sim 0.3$ Å^{-1} in the pH range 2.4−3.1 at 20 °C does not show the pH dependence, indicating that the intramolecular structure of HEWL, namely the inter-domain correlation and the polypeptide arrangement, mostly holds in the real-space resolution $d \sim 10$ Å where $d = 2\pi/q_{max}$ and the observed maximum value q_{max} is 0.6 Å^{-1}. At every pH the Kratky plot in the q range of 0.3−0.6 Å^{-1} varies gradually with elevating the temperature, reflecting that the intramolecular structural change starts from the lowest temperature. The Kratky plot alters its profile from a curve with a broad hump at around $q \sim 0.4$ Å^{-1} to an asymptotic slope, indicating that the polypeptide conformation loses a persistence of curvature to form a persistent chain with only a persistence of direction (so-called Kratky−Porod chain). In other words, the thermal denaturation of HEWL proceeds gradually in the intramolecular structure by losing rigidity of the polypeptide chain curvature. However, even at the highest temperature the polypeptide conformation is not a Gaussian-chain conformation but a persistent-chain one. The presence of the broad peaks at around $q \sim 0.1$ Å^{-1} in the Kratky plots shows that the HEWL molecules hold some compactness of the tertiary structure even at highest temperature.[34,35] The drastic changes of the broad peaks in the Kratky plots start from higher temperature in comparison with the gradual changes of the Kratky plots in the q range of 0.3−0.6 Å^{-1}, indicating that the intramolecular structural change proceeds gradually, such as a second-order transition, and that the tertiary structural change occurs, such as a first-order transition. The appearance of the subsidiary peak at around $q \sim 0.04$ Å^{-1} results from an aggregation caused by the thermal denaturation of HEWL molecules under the present solvent condition.

On the other hand, in Figures 3 and 4 the marked changes in both the $p(r)$ function and the radius of gyration R_g, obtained by using eqs 1 and 4, start from a much higher temperature compared with the gradual change of the intramolecular structure which was discussed above. This suggests that the tertiary structural change in shape and dimension proceeds after the intramolecular structural change. In Figure 3 the $p(r)$ profile changes from a bell-shape at 20 °C to a tailed-shape at higher temperatures, indicating an expansion of the molecular structure with the elevation of temperature. The maximum particle dimension D_{max}, estimated from the $p(r)$ function ($p(r) = 0$ for $r > D_{max}$), increases remarkably, which also indicates significant thermal expansion of the tertiary structure. The temperature where the significant change in the $p(r)$ profile and the D_{max} value occur moves to lower temperature with lowering pH. The beginning temperature of the change of R_g in Figure 4 shows an evident pH dependence, namely, around 48 °C at pH 2.4, 53 °C at pH 2.8, and 58 °C at pH 3.1. The above temperature, reflecting the start of the marked tertiary structural change, well corresponds to the onset temperature of the change of the heat capacity function $C(T)$ determined from the observed DSC thermogram shown in Figure 5, where we carried out the DSC measurements of the HEWL samples prepared under the same conditions used for the scattering measurements to compare the SAXS results with the DSC ones directly. The onset temperatures observed by the DSC measurements are 48.1 °C at pH

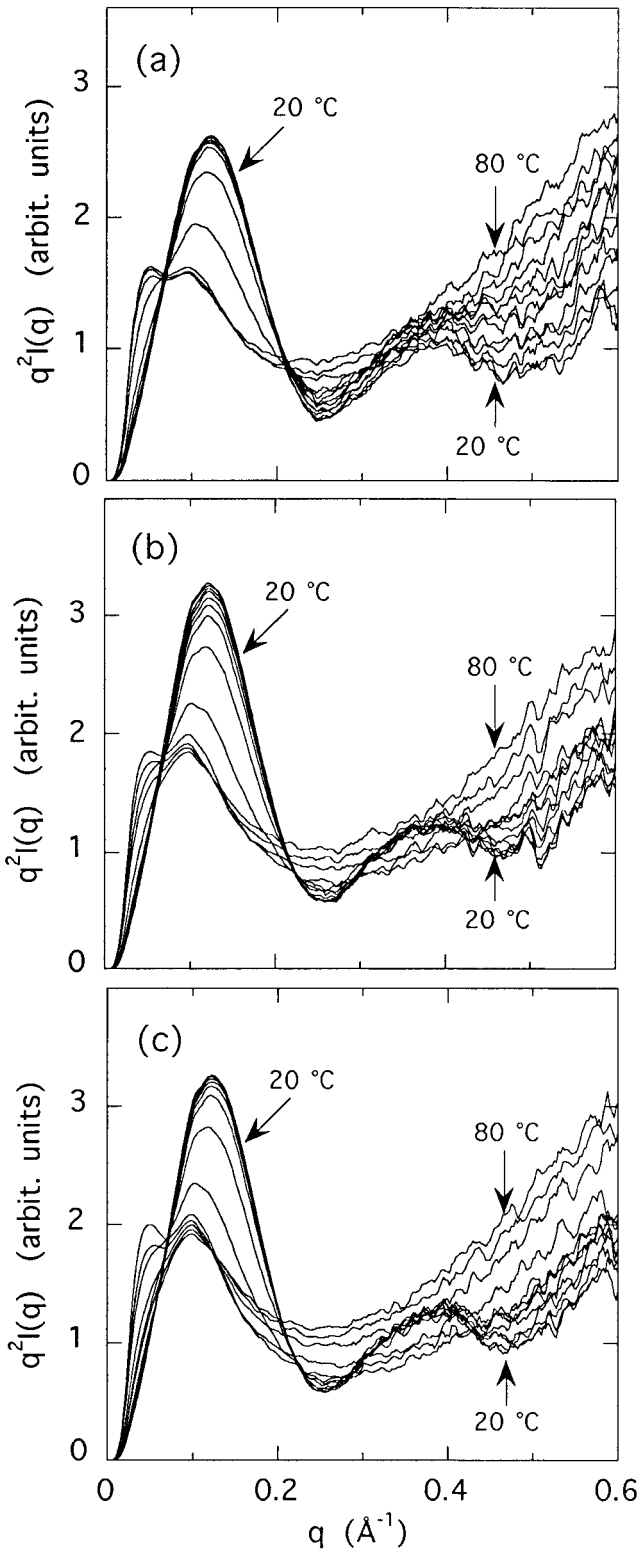

Figure 2. Variation of the Kratky plots ($q^2I(q)$ vs. q plots) of the scattering curves $I(q)$ in Figure 1. Parts (a), (b), and (c) are as in Figure 1. The changes of the Kratky plots for each 5 °C rise in temperature are presented.

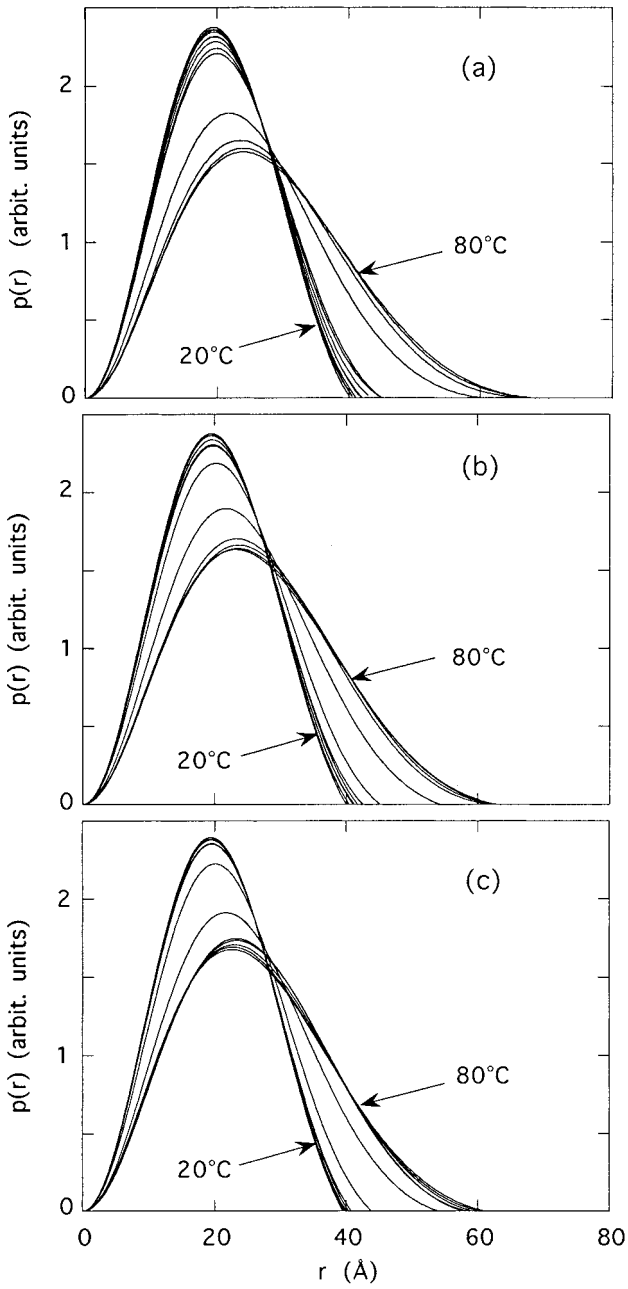

Figure 3. Distance distribution functions $p(r)$ at different pH values depending on temperature. The $p(r)$ functions were obtained by the Fourier transform of the scattering curves $I(q)$ in Figure 1. Parts (a), (b), and (c) are as in Figure 1. The changes of the $p(r)$ functions for each 5 °C rise in temperature are presented.

2.4, 54.2 °C at pH 2.8, and 57.0 °C at pH 3.1, respectively. The calorimetric enthalpy change ΔH^{cal} is 337 ± 35 kJ/mol at pH 2.4, 329 ± 30 kJ/mol at pH 2.8, and 336 ± 30 kJ/mol at pH 3.1, respectively. The above thermodynamic parameters differ slightly from those reported in the previous works,[4−6,9] which would be attributable to the experimental conditions such as the scanning rate or the solute concentration in DSC measurements. However, those differences in thermodynamic parameters do not affect the above discussion essentially, as we showed previously.[18] Then we can understand that the thermal expansion, namely the collapse of the tertiary structure of HEWL, involves a great heat capacity change, as also suggested previously by using standard scattering data analyses and DSC data.[18,19]

Complementary Analyses of Scattering and DSC Data on Transition Multiplicity. To analyze a multiplicity of structural transition from SAXS data in another way, we applied the following equation to the scattering profiles in a defined q range of q_1-q_2 Å^{-1} as given by

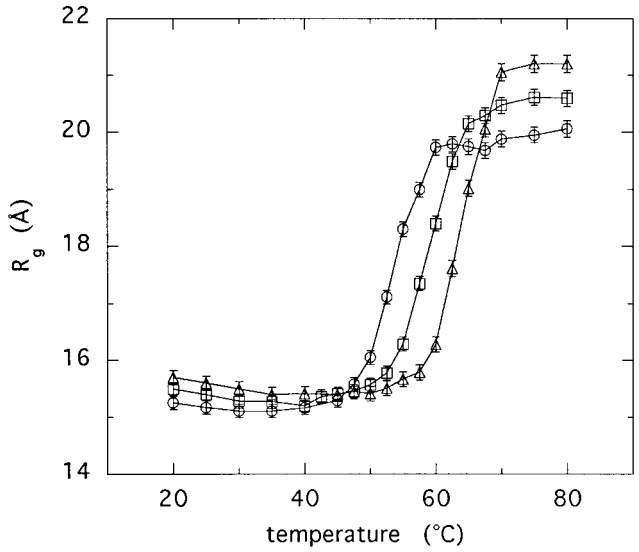

Figure 4. Temperature dependence of the gyration radii R_g at different pH values determined by the Glatter method. Parts (a), (b), and (c) are as in Figure 1. ○ at pH 2.4; □ at pH 2.8; △ at pH 3.1.

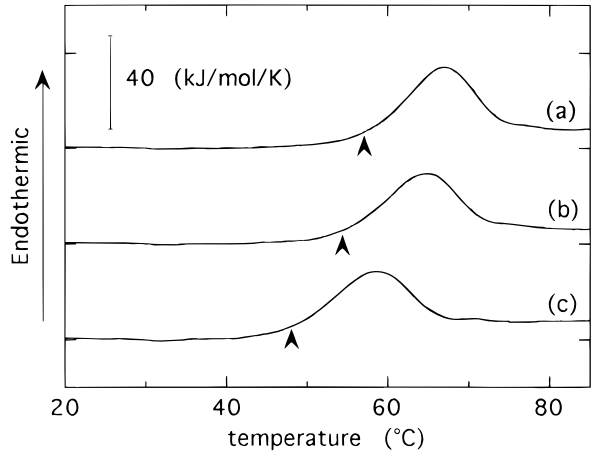

Figure 5. Differential scanning calorimetry thermograms of the hen egg-white lysozyme solutions in citrate buffer at different pH: (a) at pH 3.1; (b) at pH 2.8; (c) at pH 2.4. The arrows indicate the onset temperatures. These solutions were prepared in the same way as those used for the scattering measurements in Figure 1.

$$\Delta = \sum_{q=q_1}^{q_2} |I(q,T)/\sum_{q=q_1}^{q_2} I(q,T) - \{\alpha I(q,T_N)/\sum_{q=q_1}^{q_2} I(q,T_N) + (1-\alpha) I(q,T_U)/\sum_{q=q_1}^{q_2} I(q,T_U)\}| \quad (5)$$

where $I(q,T_N)$, $I(q,T_U)$ and $I(q,T)$ are the scattering profiles at the initial, final, and intermediate temperatures (T_N,T_U, and T), respectively. Under a two-state structural transition hypothesis the factors of α and (1−α) correspond to the molar fractions of the initial and final temperature states at T when the $I(q,T)$ profile in the defined q range is fitted by using the $I(q,T_N)$ and $I(q,T_U)$ profiles. The molar fraction α in a defined q range at an intermediate temperature was determined to give a minimum value of Δ in eq 5. Δ represents the deviation factor in the above fitting, namely the deviation from the two-state structural transition hypothesis, meaning an indication of the multiplicity of spatial-conformational-state transition. Alternatively, this method using eq 5, which we call transition-multiplicity analysis (TMA) from now on, means that the scattering curve in a defined q region at an intermediate temperature is fitted by using the two scattering curves at the initial and final temperatures since in a defined q region we normalize each scattering curve by the integrated scattering intensity in this q region. Here we assumed that at equilibrium the unfolding transition of HEWL can be described by a population of the HEWL proteins with folded (N-state) and unfolded (U-state) stages. In the present case the HEWL molecules at an intermediate temperature T were assumed to take spatial-conformations given by a population of the spatial-conformations at the initial and final temperatures (T_N = 20 °C, T_U = 80 °C), where the molar fraction α of $I(q,T_N)$ was given to be 1 at 20 °C and 0 at 80 °C. The above assumption is evidently comparable with the application of the van't Hoff equation to scanning calorimetry analyses for a two-state transition.[5] By using this equation we also evaluated an apparent value of the molar fraction of the native state at an intermediate temperature from the observed DSC thermograms.

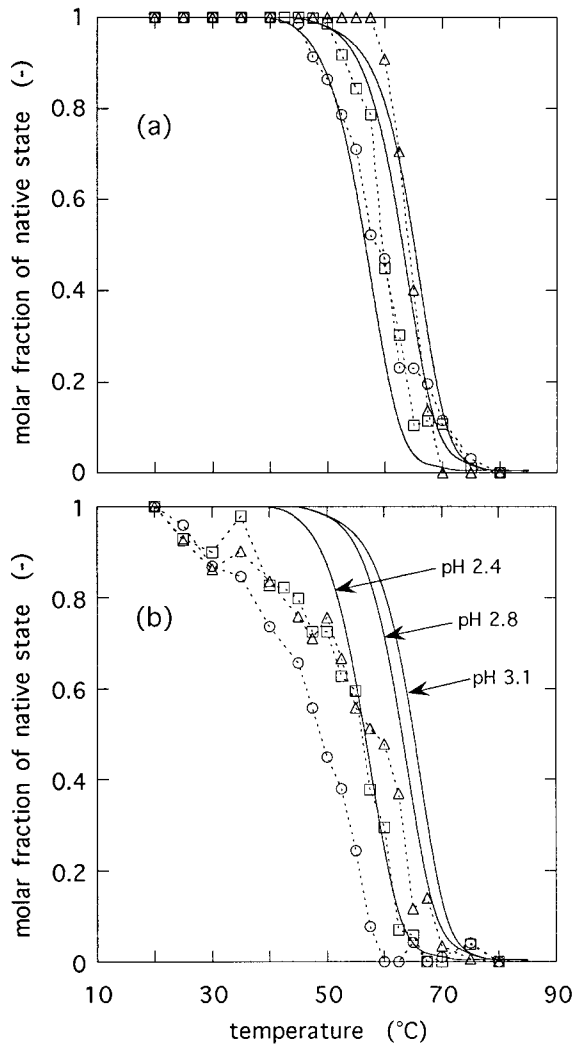

Figure 6. Comparison of the molar fraction determined from DSC data with the molar fractions determined from SAXS data in two different q ranges, namely, (a), in a q range of 0.1−0.2 Å^{-1}; (b), in a q range of 0.3−0.5 Å^{-1}. The molar fractions obtained from SAXS data in (a) and (b) reflect the molar fractions at intermediate temperatures between the tertiary structures at initial and final temperature states and those between the intramolecular structures at initial and final temperature states, respectively. In (a) and (b) the full lines represent the molar fractions determined from DSC, and the dotted lines with marks represent the molar fractions determined from SAXS. The marks ○, □, and △ are as in Figure 4.

Figure 6 shows the temperature dependence of the molar fractions at different pH values, where the full lines correspond

to the molar fractions obtained from DSC thermograms in Figure 5, and the dotted lines correspond to the molar fractions obtained from the TMA method using SAXS data in different q ranges; (a), 0.1−0.2 Å^{-1}; (b), 0.3−0.5 Å^{-1}, respectively. As explained in Figure 1, the molar fraction in the q range of 0.1−0.2 Å^{-1} in Figure 6a mostly corresponds to that of the initial spatial-conformational state of the tertiary structure at an intermediate temperature. The molar fraction in the q range of 0.3−0.5 Å^{-1} in Figure 6b corresponds to that of the initial spatial-conformational state of the intramolecular structure at an intermediate temperature. As shown in Figure 6a, the changing tendency of the molar fraction of the tertiary structure mostly agrees with that from DSC data. With lowering pH the transition-midpoint temperature of the molar fraction of the tertiary structure gradually shifts from ∼64 to ∼58 °C, and in the case of the molar fractions from DSC the transition-midpoint temperature shifts from 64.9 to 56.3 °C. This indicates that the significant change of the tertiary structure accompanies a large heat absorption observed by DSC. On the other hand, in Figure 6b the molar fraction of the intramolecular structure deviates significantly from that obtained from DSC data, namely the transition-midpoint temperature of the molar fraction of the intramolecular structure shifts from ∼57 to ∼48 °C. This clearly shows that the change of the intramolecular structure starts from a much lower temperature compared with the above main-transition temperature of the tertiary structure, meaning that a pre-transition of the intramolecular structure can proceed with a rather minor change of free energy which was unobservable under the present DSC measurement conditions.

Figure 7 shows the temperature dependence of the deviation factor Δ for the optimized α factor in Figure 6. With elevating temperature the factor Δ of the intramolecular structure fluctuates around a relatively large value of ∼0.06, which does not show any pH or temperature dependence, indicating that the feature of the thermal spatial-conformational transition of the intramolecular structure deviates from the simple two-state structural transition hypothesis over the measured temperature range at all pH values. On the other hand, the factor Δ of the tertiary structure evidently depends on both pH and temperature. Namely, the factor Δ of the tertiary structure takes a maximum value around the midpoint of the DSC thermogram in Figure 5, and by lowering the pH from 3.1 to 2.4 the temperature of the maximum value shifts to a lower temperature with an accompanying broadening of the peak width and an increase in the peak height in factor Δ. This suggests that the deviation from the two-state structural transition feature in the tertiary structural change at pH 2.4 is much enhanced around the transition temperature compared with that at pH 3.1, alternatively, that the thermal spatial-conformational transition of the tertiary structure of HEWL tends to proceed through multiple pathways as the pH is lowered from 3.1 to 2.4.

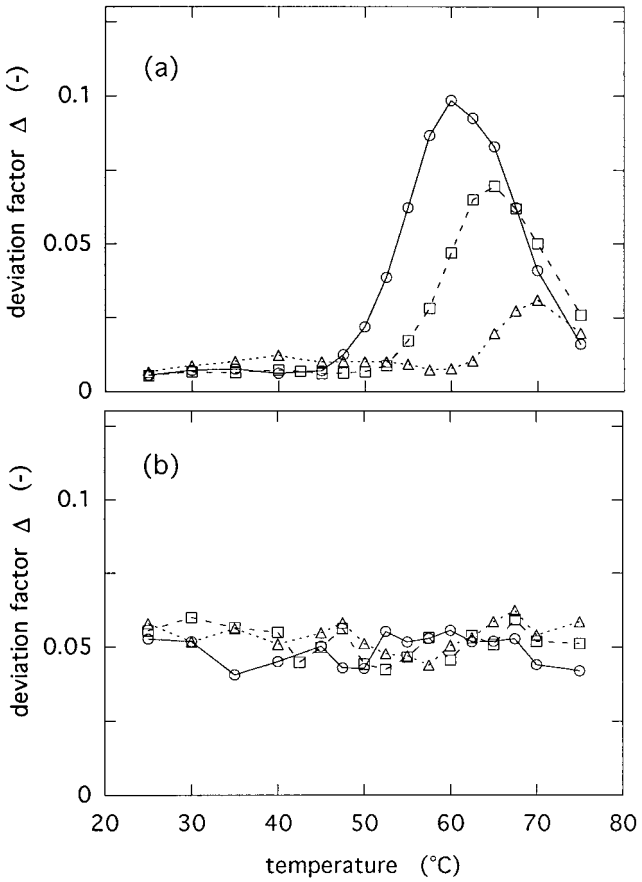

Figure 7. Temperature dependence of the deviation factors for the optimized values of the molar fractions determined from SAXS in Figure 6. Parts (a) and (b) correspond to the two different q ranges of 0.1−0.2 Å^{-1} and 0.3−0.5 Å^{-1}, respectively, as in Figure 6. The marks ○, □, and △ are as in Figure 4.

Discussion

SAXS and DSC measurements afford us complementary information of thermal denaturation of proteins from two different viewpoints of spatial-conformational-state transition and of thermodynamic-microstate transition, respectively. In the above standard SAXS-data analyses, the marked changes of the distance distribution function $p(r)$ and of the radius of gyration R_g coincide well with the onset and midpoint temperatures observed by DSC, suggesting that in the case of HEWL the thermal spatial-conformational-state transition in long spatial distance (the major collapse of the tertiary structure) involves the thermodynamic-microstate transition with a significant change of Gibbs free energy. The Kratky-plot analysis shows that the spatial-conformational-state transition in short spatial-distance (the change of the intramolecular structure) continuously proceeds without or with a minor change of Gibbs free energy prior to the major collapse. In addition to the above results, which essentially agree with our previous results treating HEWL at the pH range 7.0−1.2,[18,19] we have successfully clarified the following detailed new features of thermal spatial-conformational-state transition of HEWL at the narrow pH range 3.1−2.4.

On the basis of the two-state transition model we have presented a new profile-fitting method of SAXS data (called TMA) to deduce the temperature dependence of the molar fraction between the low- and high-temperature spatial-conformational states, namely the molar fraction between native and denatured conformational states at an intermediate temperature. The molar fraction obtained by the TMA method can be compared with that of the thermodynamic microstates obtained by applying the van't Hoff equation to DSC data under the scheme of the two-state transition which is widely used. We have found that the conformational states in long spatial-distance (tertiary structure and its collapse) are strongly coupled to the thermodynamic microstates observed by DSC, while that those in short spatial-distance (intramolecular structure and its fluctuation) do so rather weakly. Namely, in the present case the transition-midpoint temperature of the tertiary structure obtained from the molar fractions in the TMA method mostly agrees with that from DSC data, and both transition-midpoint temperatures show similar pH dependence. The molar fractions of the

intramolecular structure are significantly different from those obtained from DSC data both in temperature dependence and in the transition-midpoint temperature. The deviation factor in the TMA method well dissects a multiplicity of spatial-conformational-state transitions to examine how the spatial-conformational-state transition deviates from the two-state transition model in the thermal denaturation process. In the present case the spatial-conformational-state transition of the tertiary structure is essentially described by the two-state transition with a sharp critical temperature in comparison with that of the intramolecular structure; however, the former transition deviates from the two-state transition feature to a multi-state one with lowering pH from 3.1 to 2.4, which shows a maximum deviation from the two-state transition feature around the transition temperature at pH 2.4. On the other hand, the thermal spatial-conformational-state transition of the intramolecular structure proceeds continuously, showing a relatively large deviation in the whole temperature range measured. In other words, the TMA method has classified the aspects of the thermal spatial-conformational-state transition feature depending on structural hierarchy. The above results clearly show that the intramolecular structural change in the interdomain correlation and in the polypeptide arrangement is gradually induced long before the drastic collapse of the tertiary structure and that such an intramolecular structural change does not obey a simple first-order transition with an intensive heat-absorption but a higher-order transition. This would relate to the previous evidences of multiple pathways in folding observed in two distinct folding domains of HEWL.[13−16]

The TMA method would present some experimental criterion for theoretical approaches to solve folding and unfolding mechanism of proteins combined with structural energetics of the molten globule state.[23,36,37] Recent theoretical studies of protein folding using three-dimensional lattice models and Monte Carlo simulations characterized the folding ability of polypeptide chains (chain consisting of N connected beads) in terms of two intrinsic characteristic temperatures.[38,39] One of them is the collapse transition temperature T_θ, above which the chain takes an extended random coil structure, the other is the folding transition temperature T_f, below which the chain takes a folded structure. Using a single parameter σ defined by $\sigma = |T_\theta - T_f|/T_\theta$ the authors classified the folding kinetics of proteins, namely fast folders for $\sigma < 0.1$, moderate folders for $0.1 < \sigma < 0.6$, and slow folders for $\sigma > 0.6$. In the above theoretical works, for $\sigma = 0.4$ and $N = 27$, T_θ and T_f roughly estimated are given $T_\theta = 36$ °C assuming $T_f \sim 60$ °C. The above lattice-model picture would be very important to understand qualitatively the present results that the thermal structural transition of HEWL is characterized mostly in terms of two different spatial-conformational-state transitions in the tertiary and intramolecular structures. If the transition-midpoint temperatures of the molar fractions determined by the TMA using the SAXS data in the different q ranges correspond to the above intrinsic characteristic temperatures, the σ values turn out to be 0.17 at pH 2.4 and 0.11 at pH 3.1. Then the HEWL in the present experimental condition can be classified as a moderate folder under their theoretical framework. The quantitative difference between our experimental and their simulation results can be explained by the authors' statements that the boundary between the categories of folding sequences depends crucially on the number N and on the model.[39] Actually, in their simulations the numbers of N were given to be 15 and 27, whereas the HEWL molecule is composed of 129 amino acid residues which form two structural domains. Folding-and-unfolding kinetics of proteins greatly depends on the number of amino acid residues, namely many proteins with amino acid residues above ~100 have been shown experimentally not to obey a simple two-state kinetics in folding-and-unfolding process as a single cooperative unit.[2] Then this difference between 129 and 27 seems to be very serious. We should consider that folding-and-unfolding kinetics also depend on if proteins are composed of a single domain or multidomains and on the inherent structural-stability of each domain. In addition, the Kratky-plot analysis shows that in the present experimental condition the HEWL did not reach a fully denatured random coil state even at the highest temperature. Although there remain such problems to be clarified, we expect that the TMA method of SAXS would serve as an experimental criterion for theoretical approaches such as lattice-model simulations supporting nucleation-collapse mechanisms of folding-and-unfolding kinetics of proteins.

Finally, we should cite recent SAXS studies treating unfolding-and-refolding of HEWL at pH 2.9 in the presence of urea.[40,41] In those studies the authors presented a singular value decomposition (SVD) method for SAXS data to analyze successfully intermediate states in unfolding and refolding processes, where they used the radius of gyration R_g obtained from the Guinier approximation using SAXS data in the small q region from 0.028 to 0.06 Å^{-1}. Clearly the SVD method is very applicable to solutions which are highly homogeneous and free of associative components, as stated by the authors.[40] However, thermal denaturation of proteins accompanies a great tendency of aggregation in many cases, which is the case for the present experiments. The use of the Guinier approximation for determining R_g is known to easily accompany inherent systematic errors caused by change of interparticle interaction. In the present case, as the scattering curves below $q \sim 0.1$ Å^{-1} were evidently affected by the change of interparticle interaction, the SVD using R_g values from the Guinier plot in the above small-angle region is inapplicable. Therefore we used the Glatter's method to reduce such artifacts for estimating R_g by using wide-q-range SAXS data. Even for our case, the TMA method is applicable to analyze SAXS data in a wide q-range and to clarify transition multiplicity not only of molecular shape and dimension (reflected in R_g values) but also of intraparticle structures. This characteristic is a major difference between the TMA and SVD methods. Here we should mention the theoretical and experimental bases of our method from the solution scattering principle. As shown theoretically,[42] the scattering function of a solute particle is known to be composed of three basic scattering functions, namely the scattering functions from a particle shape, from an intraparticle structure, and from those cross-term. A previous neutron scattering study treating HEWL gives an experimental example for the separation of the above basic scattering functions,[43] where the scattering functions below $q \sim 0.2$ Å^{-1} and above $q \sim 0.3$ Å^{-1} mostly reflect the molecular shape and intramolecular structure, respectively. According to such theoretical and experimental bases, we have developed the present TMA method. We are now continuing further experiments to confirm the multiplicity of thermal transition depending on the structural hierarchy and stability of other proteins by using the TMA method.

Acknowledgment. We thank Prof. Takizawa of Gunma University for fruitful discussion on DSC measurements and Dr. K. Kobayashi of the Photon Factory at the National Laboratory for High Energy Physics for his help with the small-angle scattering instrumentation. This work was performed under

the approval of the Photon Factory Program Advisory Committee (Proposal No. 95G094 & 98G186).

References and Notes

(1) *Protein Folding*; Creighton, E. E., Ed.; W. H. Freeman & Co.: New York, 1992.
(2) *Mechanisms of Protein Folding*; Pain, R. H., Ed.; Oxford University Press: New York, 1994.
(3) Tanford, C. *Adv. Protein Chem.* **1968**, *23*, 121.
(4) Tanford, C. *Adv. Protein Chem.* **1970**, *24*, 1.
(5) Privalov, P. L.; Khechinashvili, N. N. *J. Mol. Biol.* **1974**, *86*, 665.
(6) Pfeil, W.; Privalov, P. L. *Biophys. Chem.* **1976**, *4*, 23.
(7) Pfeil, W.; Privalov, P. L. *Biophys. Chem.* **1976**, *4*, 33.
(8) Pfeil, W.; Privalov, P. L. *Biophys. Chem.* **1976**, *4*, 41.
(9) Privalov, P. L.; Gill, S. J. *Adv. Protein Chem.* **1988**, *39*, 191.
(10) Privalov, P. L. *Annu. Rev. Biophys. Chem.* **1989**, *18*, 47
(11) Tanford, C.; Aune, K. C.; Ikai, I. *J. Mol. Biol.* **1973**, *73*, 185.
(12) Kuwajima, K. *Proteins: Struct. Funct. Genet.* **1989**, *6*, 87.
(13) Miranker, A.; Radford, S. E.; Karplus, M.; Dobson, C. M. *Nature* **1991**, *349*, 633.
(14) Radford, S. E.; Dobson, C. M.; Evans, P. A. *Nature* **1992**, *358*, 302.
(15) Radford, S. E.; Buch, M.; Topping, K. D.; Dobson, C. M.; Evans, P. A. *Proteins* **1992**, *14*, 237.
(16) Buck, M.; Radford S. E.; Dobson, C. M. *Biochemistry* **1993**, *32*, 669.
(17) Privalov, G.; Kavina, V.; Freire, E.; Privalov, P. L. *Anal. Biochem.* **1995**, *232*, 79.
(18) Hirai, M.; Arai, S.; Iwase, H.; Takizawa, T. *J. Phys. Chem.* **1998**, *102*, 1308.
(19) Hirai, M.; Arai, M.; Iwase, H.; Takizawa, T.; Shimizu, S.; Furusaka, M. *Physica B*, **1998**, *241*−*243*, 1159.
(20) Filimonov, V. V.; Potekhin, S. A.; Matveev, S. V.; Privalov, P. L. *J. Mol. Biol.* **1982**, *16*, 435.
(21) Kidokoro, S.; Wada, A. *Bioplymers* **1987**, *26*, 213.
(22) Kidokoro, S.; Uedaira, H.; Wada, A. *Biopolymers* **1988**, *27*, 271.
(23) Hilsner, V. J.; Freire, E. *J. Mol. Biol.* **1996**, *262*, 756.
(24) Lattman, E. E. *Curr. Opin. Struct. Biol.* **1994**, *4*, 87−92.
(25) Kataoka, M.; Goto, Y. *Folding Des.* **1996**, *1*, R107.
(26) Ueki, T.; Hiragi, Y.; Kataoka, M.; Inoko, Y.; Amemiya, Y.; Izumi, Y.; Tagawa, H.; Muroga, Y. *Biophys. Chem.* **1985**, *23*, 115.
(27) Feigin, L. A.; Svergun, D. I. In *Structure Analysis by Small-Angle X-ray and Neutron Scattering*; Taylor, G. W., Ed.; Plenum Press: New York, 1987; p 68.
(28) Porod, G. *Kolloid Z.* 1951, *124*, 83.
(29) Kratky, O.; Porod, G. *Recl. Trav. Chim. Pays-Bas* **1949**, *68*, 1106.
(30) Kriste, R. G. *Makromol. Chem.* **1967**, *101*, 91.
(31) Kriste, R. G.; Oberthür, R. C. In *Small-Angle X-ray Scattering*; Glatter, O., Kratky, O., Eds.; Academic Press: London, 1982; p 387.
(32) Hirai, M.; Hirai, T.; Ueki, T. *Makromol. Chem.* **1993**, *194*, 2885.
(33) Hirai, M.; Hirai, T.; Ueki, T. *Polymer* **1994**, *35*, 2222.
(34) Lattman, E. E. *Cuurent Opin. Struct. Biol.* **1994**, *4*, 87.
(35) Doniach, S.; Bascle, J.; Garel, T.; Orland, H. *J. Mol. Biol.* **1995**, *254*, 960.
(36) Mark, A. E.; Gunsteren, W. F. *Biochemistry* **1992**, *31*, 7745.
(37) Haynie, D. T.; Freire, E. *Proteins: Struct. Funct. Genet.* **1993**, *16*, 115.
(38) Klimov, D. K.; Thirumalai, D. *Phys. Rev. Lett.* **1996**, *76*, 4070.
(39) Klimov, D. K.; Thirumalai, D. *Proteins: Struct. Funct. Genet.* **1996**, *26*, 411.
(40) Chen, L.; Hodgson, K. O.; Doniach, S. *J. Mol. Biol.* **1996**, *261*, 658.
(41) Chen, L.; Wildegger, G.; Kiefhaber, T.; Hodgson, K. O.; Doniach, S. *J. Mol. Biol.* **1996**, *261*, 658.
(42) Stuhrmann, H. B.; Miller, A. *J. Appl. Crystallogr.* **1978**, *11*, 325.
(43) Stuhrmann, H. B.; Fuess, H. *Acta Crystallogr.* **1976**, *A32*, 67.